CHAPTER TWO

Specimen Behavior in the Electron Beam

R.M. Glaeser[1]
Lawrence Berkeley National Laboratory, University of California, Berkeley, CA, United States
[1]Corresponding author: e-mail address: rmglaeser@lbl.gov

Contents

1. Introduction 20
2. High-Energy Electrons Are a Form of Ionizing Radiation as Well as Being a Form of Short-Wavelength Radiation That Can Be Focused 21
   - 2.1 Electron-Scattering Events Can Be Either Elastic or Inelastic 21
   - 2.2 Energy Is Deposited in the Specimen as a Result of Inelastic Scattering 22
   - 2.3 Values of the Linear Energy Transfer (LET) Can Be Used to Estimate the Energy Deposited 24
3. Biological Molecules Become Structurally Damaged When Irradiated 25
   - 3.1 There Is a Large Literature of Radiation Chemistry and Radiation Biology 25
   - 3.2 Fading of Diffraction Patterns Is a Convenient Indicator of Structural Damage 27
   - 3.3 Some Residues in Proteins Are Especially Sensitive to Radiation Damage 28
   - 3.4 Caging of Fragments and "Trapping" of Radicals Results in Cryo-Protection: This Helps Only to a Limited Extent 29
   - 3.5 Radiation Sensitivity of Enzyme Activity: Implications for Dynamic Studies in Liquid Samples 30
4. Vitreous Ice Also Becomes Structurally Damaged by Ionizing Radiation 30
   - 4.1 Water Molecules Are Easily Damaged by Ionizing Radiation 30
   - 4.2 Weak Thon Rings at High Resolution Show That Vitreous Ice Is Very Sensitive to Radiation Damage 31
   - 4.3 Electron-Stimulated Desorption Progressively Thins Ice Specimens 33
5. Bubbling of Hydrated Biological Specimens Becomes Apparent at High Electron Exposure 34
   - 5.1 Bubbles Consist of Molecular Hydrogen 35
   - 5.2 Bubbling Can Be Used to Evaluate the Specimen Thickness 36
   - 5.3 Bubbling Can Be Used to Distinguish Regions with Different Chemical Composition (Bubblegrams) 36
6. Cryo-Specimens Exhibit Collective Beam-Induced Movement When Irradiated 37
   - 6.1 Radiation-Sensitive Specimens Show Beam-Induced Motion at Quite Low Electron Exposures 37
   - 6.2 Thin Cryo-Specimens Undergo Drum-Head-Like Flexing and Doming When Irradiated 38
   - 6.3 Images Can Be Corrupted Significantly by There Being Changes in *Z*-Height 39

Methods in Enzymology, Volume 579
ISSN 0076-6879
http://dx.doi.org/10.1016/bs.mie.2016.04.010

6.4 The Pattern of Beam-Induced Movement Can Be Quite Unpredictable 39
7. More Than One Mechanism May Contribute to Beam-Induced Motion 40
7.1 Cryo-EM Specimens, as Made, Are Expected to Be Under Considerable Stress 40
7.2 Irradiation Can Relieve Mechanical Stress 41
7.3 Irradiation Can Generate (New) Mechanical Stress 41
7.4 Which Comes First, Relaxation or Creation of Stress? 42
8. Irradiation Can Produce Electrostatic Charging of the Specimen 42
8.1 A Buildup of Net Charge on the Specimen Can Be Easy to Detect 43
8.2 Evidence of Net-Charge Buildup Can Be Reduced in Several Ways 43
8.3 Other Forms of Specimen Charging Are More Subtle to Detect 44
9. Summary and Future Directions 46
Acknowledgments 47
References 47

Abstract

It has long been known that cryo-EM specimens are severely damaged by a level of electron exposure that is much lower than what is needed to obtain high-resolution images from single macromolecules. Perhaps less well appreciated in the cryo-EM literature, the vitreous ice in which samples are suspended is equally sensitivity to radiation damage. This chapter provides a review of several fundamental topics such as inelastic scattering of electrons, radiation chemistry, and radiation biology, which—together—can help one to understand why radiation damage occurs so "easily." This chapter also addresses the issue of beam-induced motion that occurs at even lower levels of electron exposure. While specimen charging may be a contributor to this motion, it is argued that both radiation-induced relief of preexisting stress and damage-induced generation of additional stress may be the dominant causes of radiation-induced movement.

1. INTRODUCTION

This chapter describes how and why cryo-EM specimens—and their images—progressively change with time as images are being recorded. The fact that electrons are ionizing radiation is the underlying, fundamental cause of such changes.

Biological specimens are easily damaged by ionizing radiation. As a result, changes in molecular structure that accumulate during the exposure are a primary concern. Ultimately, the molecular damage becomes so extensive that it is futile to extend the exposure any further.

Even at the very beginning of an exposure, it is possible that irradiating a specimen may relieve preexisting stress. At the same time, the accumulated

structural damage may also generate new stress as the exposure continues. Either way, dynamic changes in stress may result in collective (beam-induced) movement of the specimen as a whole. This specimen movement, possibly along with movement of the image caused by electrostatic charging of the specimen, causes blurring of high-resolution features of the image. It thus is important to be aware of these effects when collecting images.

2. HIGH-ENERGY ELECTRONS ARE A FORM OF IONIZING RADIATION AS WELL AS BEING A FORM OF SHORT-WAVELENGTH RADIATION THAT CAN BE FOCUSED

2.1 Electron-Scattering Events Can Be Either Elastic or Inelastic

When an incident electron is scattered by the specimen, the outcome is described as being either an elastic or an inelastic event, depending upon whether the electrons within the specimen remain in their ground state or not. The relative probabilities for elastic vs inelastic-scattering events are proportional to their respective "total scattering cross sections." The values of these cross sections depend primarily upon the atomic numbers of the atoms making up the specimen, and one can ignore the extent to which they depend upon the chemical bonding between the atoms. Section 5.2.4 in Reimer and Kohl (2008) estimates that the ratio of inelastic scattering to elastic-scattering scales theoretically as $\sim 26/Z$, where Z is the atomic number, whereas experimentally is seems to scale as $\sim 20/Z$. This difference is of minor importance. What is important is that the relative amounts of elastic and inelastic scattering are similar for different types of biological materials, differing mainly to the extent that their chemical compositions may differ.

Both the elastic and inelastic-scattering cross sections decrease strongly (roughly as $1/v^2$, where v is the electron speed) as the energy of the incident electrons increases. The decrease in the elastic-scattering cross section, at higher voltage, leads to a decrease in the contrast of weak phase objects, of course. At the same time, however, the decrease in the inelastic-scattering cross section makes it possible to use a correspondingly larger electron exposure, while still staying within the same limit of what is a "safe" radiation dose.

The ratio of elastic to inelastic-scattering cross sections for carbon decreases by only $\sim$13% as the energy of the incident electrons is increased from 100 to 300 keV, as can be calculated from equation 5.65 in Reimer and

Kohl (2008). As a result, the signal-to-noise ratio in the image does not change significantly as the voltage is increased, provided that one takes advantage of the increased electron exposures that are allowed at higher voltages, as is mentioned in the previous paragraph.

On the other hand, there are incremental benefits that come with using higher electron energies, such as the fact that the depth of focus increases in inverse proportion to the electron wavelength. The depth of focus relative to the thickness of the sample becomes increasingly important as the image resolution improves (Agard, Cheng, Glaeser, & Subramaniam, 2014). Another consideration, important at all resolutions, is that plural scattering decreases as the voltage increases. More specifically, there is a smaller loss of signal due to some of the (single-scattering) elastic events being either preceded by, or followed by, one or more inelastic events. The extent to which this type of plural scattering is important depends upon the ratio of the sample thickness relative to the mean-free path for inelastic scattering. For samples much thinner than the mean-free path, a fraction t/Λ of the elastically scattered electrons are lost to a second, inelastic event, where t is the sample thickness, and Λ is the mean-free path. Perhaps the best estimate for the inelastic mean-free path in ice is ~200 nm at an energy of 120 keV (Grimm, Typke, Barmann, & Baumeister, 1996). This value, in turn, suggests that the mean-free path for inelastic scattering of 300 keV electrons is ~350 nm.

2.2 Energy Is Deposited in the Specimen as a Result of Inelastic Scattering

Variable amounts of energy are lost by incident, high-energy electrons as a result of individual, inelastic-scattering events. Most of this energy is deposited within the specimen, and only a small fraction is carried away in the form of the kinetic energy of secondary electrons.

When the amount of energy lost in individual scattering events is measured for a large number of electrons, the probabilities for various energy losses can be presented as an energy-loss spectrum. Fig. 1, reproduced from Aronova and Leapman (2012), shows examples of such spectra for a few, representative biological materials.

If the specimen is thin enough, most of the electrons remain unscattered. These unscattered electrons make up the majority of the large peak that is seen at zero energy loss in Fig. 1B. The elastically scattered electrons also show up in the zero-loss peak, of course.

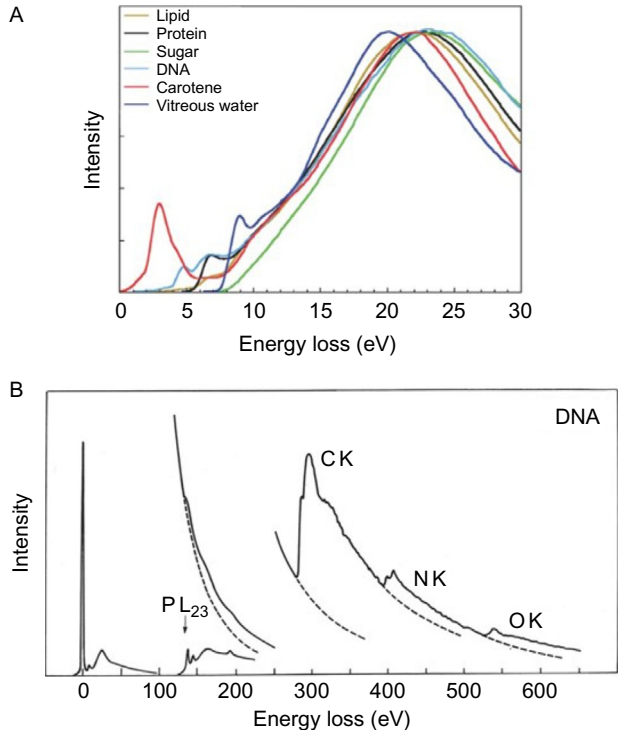

Fig. 1 Electron energy-loss spectra of various biological materials. Panel (A) shows just the region of low energy losses, from 0 to 30 eV. The various energy-loss peaks produced by different materials in the region 0–10 eV correspond to peaks in the UV–vis spectra of the same materials. The broad, intense peak extending from about 10 eV to almost 100 eV is due to the "plasmon" loss, or collective dielectric loss of the materials. Plasmon losses have limited usefulness to distinguish different types of biological materials. They are, on the other hand, the main events that lead to ionization and radiation damage of biological materials. Panel (B) shows a broader range of the energy-loss spectrum for DNA. Various peaks are shown in the range of ~150–600 eV energy loss, corresponding to inner-shell ionization energies of various elements. *Reproduced with permission from Aronova, M. A., & Leapman, R. D. (2012). Development of electron energy loss spectroscopy in the biological sciences.* MRS Bulletin/Materials Research Society, 37*(1), 53–62. doi: 10.1557/mrs.2011.329.*

Different regions of the energy-loss spectrum correspond to quite different physical events. Peaks in the spectrum at energies below about 10 eV, seen in some of the curves in Fig. 1A, correspond to peaks in the optical absorption (UV–vis) spectrum. This part of the (energy-loss) spectrum is mainly associated with single-electron excitations of conjugated bond systems, such as aromatic groups or linear polyenes.

The large, broad peak between 10 and 100 eV, seen for all materials, corresponds to the simultaneous (collective) excitation of many electrons in the specimen. In metals, the process is referred to as plasmon excitation. The same terminology is often used even when the specimen is not a metallic conductor. Alternatively, this collective excitation can be called a "dielectric loss." In an insulator, excitation of a mode in which many electrons move in synchrony soon decays into lower energy, single-electron excitations and ionizations, plus heat. Such single-electron ionization events are very likely to result in radiolysis of aliphatic organic molecules, while aromatic molecules—as we know empirically—are much less likely to be damaged. The distinction, of course, is that the loss of a single valence electron is localized to a single bond in aliphatic molecules, while in an aromatic molecule the loss is delocalized over multiple covalent bonds.

Finally, in the energy-loss range of a few hundred eV (for organic molecules), there are small peaks—like those shown in Fig. 1B—that correspond to ionization of K-shell (1S-state) electrons. K-shell ionization of low-Z atoms usually decays by the Auger process (Chattarji, 1976). Such events often cause ejection of two or more valence electrons from a single atom. As a result, K-shell ionization is very likely to result in bond rupture, even for aromatic molecules. The relative frequency of such events is low, however, since the cross section for K-shell ionization is about 1000 times smaller than for plasmon excitation. The net result is that K-shell ionization makes a negligible contribution to radiation damage at the electron exposures used in cryo-EM.

2.3 Values of the Linear Energy Transfer (LET) Can Be Used to Estimate the Energy Deposited

The term "linear energy transfer (LET)" is used to indicate the average amount of energy that is lost per unit path-length as a charged particle travels through a given material. The LET for electrons is traditionally expressed in units of MeV/cm, or, when divided by the mass density, in units of MeV-cm^2/g. Values of the LET for electrons have been tabulated for many materials and for a wide range of energies of the incident electrons (Berger & Selzer, 1964).

The average amount of energy deposited in a thin sample, per electron, can be estimated by multiplying the LET by the sample thickness, t. Similarly, the total energy deposited per gram of a specimen, following an exposure of N electrons/area, is

$$E = \frac{\mathrm{LET} \cdot N}{\rho} \tag{1}$$

where ρ is the mass density of the specimen material.

The energy deposited per gram is referred to as the radiation dose. Radiation doses are usually expressed in rads in the older literature, where 1 rad is equal to 100 erg/g. Alternatively the dose is expressed in the Standard International (SI) units of gray (Gy), where 1 Gy = 1 J/kg, and thus 1 rad = 0.01 Gy. Since the dose is proportional to the electron exposure, it is commonly used jargon to refer to the exposure as being the "dose." While this terminology is not strictly correct, the intended meaning becomes understandable in context.

Taking vitreous ice as an example, the LET for 300 keV electrons, divided by the mass density, is ~2.4 MeV cm^2/g. It follows that a dose of $\sim 3.8 \times 10^9$ rad is deposited in a cryo-EM specimen as a result of an electron exposure of 10 e/$Å^2$. This estimate is too high, of course, because not all of the energy lost by incident electrons is actually deposited in a thin sample. Rather, as mentioned earlier, some of the energy escapes in the form of kinetic energy of secondary electrons. Depending upon the thickness of the specimen, the actual dose has been estimated to be reduced by half or more (Grubb, 1974). Unless one is concerned about making a very precise estimate of the radiation dose, however, it is not important to make a correction for this effect.

To further illustrate the linear relationship expressed in Eq. (1), the rad dose is plotted in Fig. 2 as a function of electron exposure. The specimen is again taken to be vitreous ice, and the energy of the electrons is assumed to be 300 keV. More is said below about each of the arrows shown in Fig. 2.

3. BIOLOGICAL MOLECULES BECOME STRUCTURALLY DAMAGED WHEN IRRADIATED

3.1 There Is a Large Literature of Radiation Chemistry and Radiation Biology

Extensive studies in radiation biology have described many effects caused by ionizing radiation. Much is known, for example, about how strand-breaks and mutations occur in DNA, even at relatively low doses (Hall & Giaccia, 2012). At ten thousand to a million-fold higher doses, even enzymatic activity is destroyed (Kempner, 1993; Kempner & Schlegel, 1979). Ultimately, at doses rarely encountered outside the context of X-ray crystallography

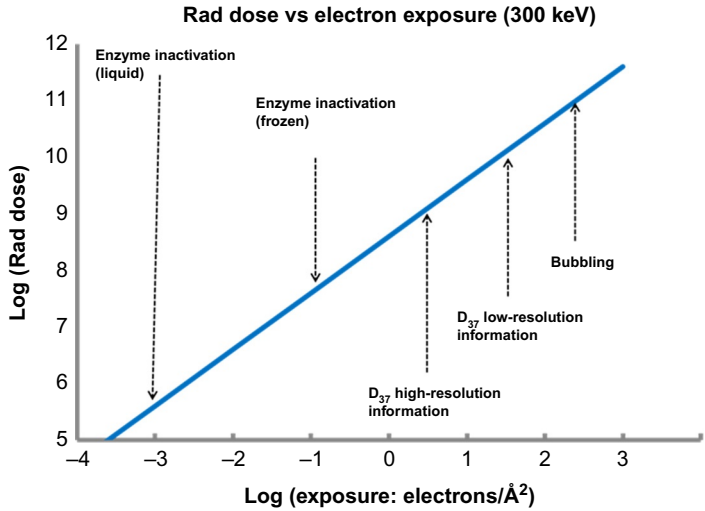

Fig. 2 Graph showing the linear relationship between electron exposure (300 keV electrons) and the rad dose deposited in a specimen. Five *annotated arrows* are included in the graph to indicate the general region of electron exposure at which various landmarks of radiation damage are incurred. The notation D_{37} indicates the dose/exposure at which the desired signal falls to 37% (e^{-1}) of its initial value.

and electron microscopy, radiation completely destroys protein structure (Howells et al., 2009).

The sensitivity of enzyme activity to radiation inactivation depends upon the size of the protein (Kempner & Schlegel, 1979), as well as upon its physical environment. As indicated in Fig. 2, for example, enzyme function may survive only up to doses $\sim 10^6$ rad when proteins are irradiated in liquid buffer, but it can survive doses as high as $\sim 10^8$ rads when frozen while being irradiated. The difference is understood to be due to the fact that many secondary chemical reactions occur in the liquid state, which cannot occur in the frozen state.

In the field of radiation chemistry, the radiolysis reaction

$$\text{Parent molecule} \xrightarrow{\text{Ionizing radiation}} \text{Products} \qquad (2)$$

is often characterized in terms of the yield, or *G*-value for the reaction. The *G*-value is defined as the "number of molecules per 100 eV" that are either destroyed or produced. One therefore speaks of *G*-values for disappearance of parent molecules, and of various *G*-values for creation of any one of the product molecules. In general, multiple different reactions of the type

indicated in Eq. (2) occur for any given parent molecule. These reactions often involve molecular fragmentation, although cross-linking and polymerization are also possible. G-values for some form of damage to the parent molecule are typically in the range of 2 or more for solid amino acids—see section 8.1 of Garrison (1968).

Biological molecules are also easily damaged by elastic events that literally knock an atom out of the molecule (Cosslett, 1970). While the large amount of momentum transfer that this requires is more favorable for a light atom than it is for a heavy atom, the Coulombic force is smaller when $Z=1$ than when $Z=6$. The net result is that knock-on events may be less likely for hydrogen atoms than they are for carbon, nitrogen, and oxygen atoms. In any case, the cross section for such "knock-on" events is very small compared to the cross section for inelastic scattering, and it is, instead, comparable to that for K-shell ionization mentioned in Section 2.2. As a result, the radiation damage caused by inelastic scattering, in particular that resulting from plasmon excitation and subsequent ionization, is far more important for biological materials than is knock-on damage. This remains the case even at very high electron energies (eg, 1–3 MeV), and even when account is taken of the displaced atom itself producing additional displaced atoms.

3.2 Fading of Diffraction Patterns Is a Convenient Indicator of Structural Damage

Electron diffraction patterns of hydrated protein crystals are easily observed in the electron microscope. These can go to quite high resolution if the crystals contain enough unit cells, and if the crystals are well ordered (Glaeser, Downing, DeRosier, Chiu, & Frank, 2007). As radiation damage begins to set in, however, the diffraction spots become progressively weaker, and the spots may also become broader. Fading of the (integrated) intensities of diffraction spots indicates that the contents of individual unit cells are becoming increasingly dissimilar, while broadening of the spots indicates that the crystal lattice is becoming less and less perfect. As is indicated in Fig. 2, high-resolution diffraction spots fade at a much faster rate than do the low-resolution spots (Baker, Smith, Bueler, & Rubinstein, 2010; Bammes, Jakana, Schmid, & Chiu, 2010; Taylor & Glaeser, 1976).

All of these phenomena are consistent with the model that radiation damage causes random structural changes in the contents of the unit cell, and the resulting structural differences first become noticeable at high resolution. An alternative interpretation would be that the crystal packing is sensitive to any change in molecular structure, even though the amounts of

structural change within the molecules themselves may be quite minor. If, for example, molecules rotate and repack within a crystal, but change little—if at all—in the process, that too might explain the fading of diffraction intensities and the broadening of diffraction spots. To the extent that this second interpretation is correct, fading of the intensities of diffraction patterns would not be an accurate way to determine the structural sensitivity of biological molecules themselves. While one can, indeed, safely assume that repacking of molecular fragments, and even whole (undamaged) molecules does occur as the electron exposure progresses, prior studies in radiation chemistry make it unreasonable to suppose that the molecules themselves remain largely undamaged.

With the recent advent of superior electron-camera technology, Grant and Grigorieff were able to estimate the fading of signal from single-particle images of a large virus. They found that there was good agreement with earlier protein-crystal data as regards the radiation sensitivity of high-resolution features (Grant & Grigorieff, 2015). As Grant and Grigorieff pointed out, however, the structure of a virus—not unlike that of a protein-crystal—is based on the packing of identical subunits. As a result, this agreement does not completely rule out the possibility that changes in subunit packing, rather than changes in subunit structure alone, contribute to fading of the high-resolution signal. In addition, Grant and Grigorieff report that the lower-resolution signal in images of this virus particle is less sensitive than it was reported to be for images of protein crystals by Baker et al. (2010). They discuss a number of alternative hypotheses that might account for the results obtained at lower resolution, but whether there is a fundamental difference in the radiation sensitivity of single particles and of protein crystals is not yet clear.

3.3 Some Residues in Proteins Are Especially Sensitive to Radiation Damage

It is well known that a few, specific amino acid residues within a protein are likely to be damaged very early, well before the diffraction intensities of the crystal have changed to a significant degree. In this regard, fading of diffraction intensities is not a sufficiently sensitive way, rather than being a too sensitive way, to determine how much electron exposure can be safely used. The residues that are likely to be damaged first include those at the active site of an enzyme, solvent-exposed disulfide bonds, and side-chain carboxyl groups.

Much of the information on this point has come from the field of protein crystallography (Weik et al., 2000). It is reasonable to ask why one should expect the effects of X-ray radiation and of electron radiation to be the same. The explanation (Henderson, 1990) is that the primary event in inelastic scattering of X-rays is the production of an electron with almost the same energy as that of the X-ray photon—either through the photoelectric effect or through Compton scattering, depending upon the energy of the photon. After that, the (moderately) high-energy electron deposits energy in the sample by exactly the same inelastic-scattering processes as occur for incident electrons in the electron microscope.

3.4 Caging of Fragments and "Trapping" of Radicals Results in Cryo-Protection: This Helps Only to a Limited Extent

When proteins are irradiated at liquid nitrogen temperature, chemical attack by reactive species such as hydroxyl radicals, which are generated by radiolysis of the surrounding buffer, is greatly reduced. As a result, only the direct effects of radiation on the macromolecule itself remain a significant cause of radiation damage (Kempner, 1993). In addition, molecular fragments produced at liquid nitrogen temperature are themselves effectively caged by their surroundings, whether that consists of adjacent solvent molecules or of adjacent parts of the macromolecule. Indeed, even free radicals produced within irradiated organic crystals do not initially participate in secondary reactions. Instead they are trapped so well by their surroundings that each time a given radical is formed, it adopts the same orientation relative to its surroundings. We thus may conclude that, even when chemical bonds are broken, the two, previously bonded atoms may, initially, still remain in van der Waals contact. It is thought that both of these effects are responsible for the significant protection effect (Glaeser & Taylor, 1978; Hayward & Glaeser, 1979) observed for proteins in cryo-EM specimens.

The desirable effects of "cryo-protection" do not continue forever as the dose continues, however. As more and more radicals form and accumulate, it becomes more and more likely that a newly trapped radical comes in van der Waals contact with a preexisting one. When that happens, the two will react spontaneously, ie, there is no activation barrier to overcome for reactions between free radicals. The resulting heat released by this favorable reaction may be sufficient to activate local rotations and displacements, thus facilitating further reactions and consequent structural disorder. This series of events can occur even when the specimen is at helium temperature. It thus is understandable that helium temperature does not provide a major

cryo-protection effect, as judged by the decay of high-resolution electron diffraction intensities, beyond that produced at nitrogen temperature (Chiu et al., 1986). A similar result has been reported for X-ray diffraction intensities of protein crystals irradiated at various temperatures, where it was found that the lifetime of high-resolution reflections did not change by more than 20% at temperatures below 100 K (see fig. 1A in Meents, Gutmann, Wagner, & Schulze-Briese, 2010). In this same study, however, specific radiation damage did show significantly greater cryo-protection, for example, that at solvent-exposed disulfide bonds (Meents et al., 2010).

3.5 Radiation Sensitivity of Enzyme Activity: Implications for Dynamic Studies in Liquid Samples

As indicated in Section 3.1, enzymes are inactivated by radiation doses of 10^6 rads or less in the liquid state. As seen in Fig. 2, this dose corresponds to an electron exposure of $\sim 2 \times 10^{-3}$ e/Å^2 or less. If two images are recorded at or above this exposure, and if the structure is observed to change between the first and the second such exposure, one can be sure that the changes are not due to some enzymatic function. Protein particles as small as ~5 nm, on the other hand, are calculated to first become detectable at an electron exposure of $\sim 2 \times 10^{-1}$ e/Å^2 under the most favorable circumstances, including the use of full phase contrast (Glaeser & Hall, 2011). There thus seems to be a large gap between what physics would allow for imaging biological specimens in the liquid state, using an environmental cell at room temperature and pressure (Ross, 2015), and what some would like to achieve.

4. VITREOUS ICE ALSO BECOMES STRUCTURALLY DAMAGED BY IONIZING RADIATION

4.1 Water Molecules Are Easily Damaged by Ionizing Radiation

Radiolytic production of hydroxyl radicals, hydrogen peroxide, and other reactive species in liquid water plays a major role in radiation biology. As a result, there is an extensive literature on the radiolysis of water and aqueous solutions (Allen, 1961; Le Caër, 2011). Fig. 3 shows a summary of the main reactions that are currently believed to occur within the first picosecond after a water molecule has been ionized (Le Caër, 2011). The yield of the final, reactive intermediates shown in Fig. 3 is actually quite high, and it might be said that water is at least as radiation-sensitive as are proteins.

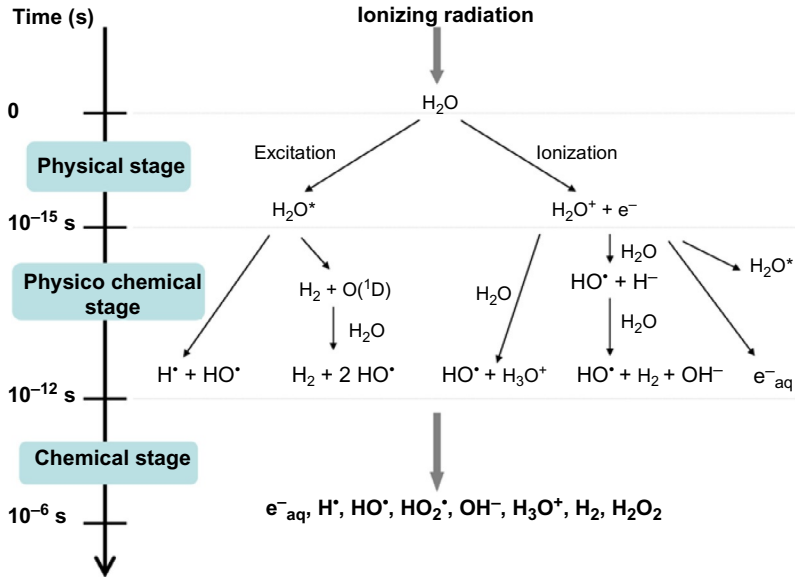

Fig. 3 Schematic progression of temporal events in the radiolysis of pure water. Products of the initial, "physical" stage of excitation and ionization evolve, within the first picosecond, to form multiple reactive intermediates such as hydrogen radicals, hydroxyl radicals, and hydrated electrons. Within a microsecond, hydrogen gas and hydrogen peroxide are among the products, as well as a number of the previously formed, reactive species. *Reproduced with permission from Le Caër, S. (2011). Water radiolysis: influence of oxide surfaces on H2 production under ionizing radiation.* Water, 3*(1), 235.*

In pure water, many of the chemical intermediates shown in Fig. 3 have no alternative but to react with each other, ultimately returning nearly everything back to molecules of water. It is even believed that hydrogen radicals and hydroxyl radicals can convert hydrogen gas and hydrogen peroxide back to water (Le Caër, 2011). This very likely is why pure ice may appear to be unchanged when irradiated in the electron microscope.

4.2 Weak Thon Rings at High Resolution Show That Vitreous Ice Is Very Sensitive to Radiation Damage

It has long been thought to be strange that images of amorphous ice—in contrast to those for graphitic, amorphous carbon—show only very weak Thon rings, if any. It now seems that two factors are involved.

At low to medium resolution, the structure factor for vitreous ice should be very weak to begin with, as it is for liquid water. The reason for this is that density fluctuations for liquid water depend only on the temperature and the

isothermal compressibility of the liquid—see eq. (1) in Clark, Hura, Teixeira, Soper, and Head-Gordon (2010). Amorphous carbon, on the other hand, is thought to have a somewhat granular, domain-like structure. In addition, the mass density of (predominantly) sp^2-bonded amorphous carbon films is two or three times greater than that of hydrogen-bonded amorphous ice. These differences all lead to much stronger structure factors, and thus stronger Thon rings, at low spatial frequencies for carbon compared to ice.

At high resolution, however, the diffraction pattern of amorphous ice, like that of liquid water, displays a strong feature known as the "water ring." One thus expects that Thon rings from ice should be especially strong at a resolution of 3–4 Å, but that is not the case.

Based on recent work by McMullan, Vinothkumar, and Henderson (2015), it now seems that radiation damage causes continual reorganization of the structural features responsible for the "water ring." As is illustrated in Fig. 4, proof that this is the case came from comparing the strength of Thon rings observed in the incoherent sum of power spectra (for successive frames

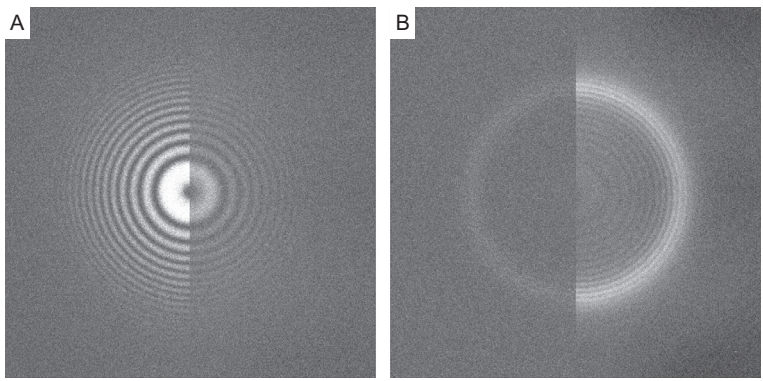

Fig. 4 Example illustrating that the power spectra of (A) amorphous carbon and (B) amorphous ice are dramatically different. In both cases images were obtained as dose-fractionated movies, using far greater electron exposures than could be tolerated by biological specimens, in order to improve the statistical definition of the power spectra. Each panel is, furthermore, split into two half-plane images in which the power spectrum of the coherent sum of frames is shown on the left half, and the "incoherent sum" of power spectra of individual frames is shown on the right half. *This figure was kindly prepared by Dr. Greg McMullan, using the same data published in McMullan, G., Vinothkumar, K. R., & Henderson, R. (2015). Thon rings from amorphous ice and implications of beam-induced Brownian motion in single particle electron cryo-microscopy.* Ultramicroscopy, 158, *26–32. doi: 10.1010/j.ultramic.2015.05.017. Republication of these data is with permission.*

of a dose-fractionated movie) to those observed in the power spectrum of the (aligned) sum of frames. If the specimen structure does not change from one frame to the next, one expects the incoherent sum of power spectra to have a lower signal-to-noise ratio (ie, the visibility of Thon rings should be less) and that was shown to be the case for a thin carbon film (see Fig. 4A). The opposite effect was seen for a thin vitreous-ice specimen; however (see Fig. 4B), leading to the conclusion that the high-resolution structure in one frame is not the same as (is not "fully coherent with") that in successive frames.

The resulting picture is that new, but equivalent structural features form in vitreous ice as the previous ones are lost due to radiation damage. In this picture, individual oxygen atoms (ie, water molecules) move significantly on the size scale of the structural organization responsible for producing the "water ring." While diffraction intensities (or power spectra) are insensitive to this reorganization, high-resolution image features are smeared out. In effect, there is a large Debye–Waller "temperature" factor (B factor) in the images, but not in the diffraction intensities.

McMullan et al. then went on to estimate that the root mean square displacement of water molecules may be ~5 Å after an exposure of 25 e/Å^2. These random, radiation-induced motions of water molecules must also jostle proteins, causing them to diffuse randomly within the vitreous ice, just as thermal motion of water molecules does in the liquid state. McMullan et al. conclude, however, that radiation-induced diffusion is unlikely to be a factor limiting the resolution attainable by single-particle cryo-EM except above ~2 Å, and then only for very small macromolecules.

4.3 Electron-Stimulated Desorption Progressively Thins Ice Specimens

It is commonly known that ice becomes progressively more transparent to the electron beam—ie, thinner, the longer that the same area is irradiated. This is actually a useful effect, as it provides a convenient way to see, when viewing the grid at low magnification (eg, in "Search" mode), where the electron beam was positioned on the specimen at the time when images were recorded at high magnification. If desired, even a complete hole can be "burned" through the ice, thereby providing a local area to accurately measure the incident electron intensity. This, in turn, makes it possible to estimate the ice thickness by making a quantitative measurement of the percent transmission of electrons in an area of interest (Agard et al., 2014).

Continuous removal of water molecules from the surface is an example of the well-known "electron-stimulated desorption" phenomenon (Ramsier & Yates, 1991). Radiation-induced thinning of ice at different temperatures was studied in detail by Heide (1984), using 100 keV electrons. He found that the rate of desorption increased steeply above 100 K, but at lower temperature, even down to 10 K, the rate remained constant. Heide reported that the rate of mass loss below 90 K corresponds to ~1 monolayer of water being removed from the surface for every 25 electrons/Å^2 of exposure. Heide also reported that the removal rate for microcrystalline cubic ice was higher than that for amorphous ice.

The amount of thinning expected for exposure to 300 keV electrons should be about half that for exposure to 100 keV electrons, ie, it should scale as the inelastic-scattering cross section. McMullan et al., on the other hand, quote a much greater rate, namely, 100 Å of ice for every 170 electrons/Å^2, attributing this estimate to Wright, Iancu, Tivol, and Jensen (2006). This discrepancy may be something that needs to be investigated further, but for most purposes, it should not affect the conduct of cryo-EM data collection.

5. BUBBLING OF HYDRATED BIOLOGICAL SPECIMENS BECOMES APPARENT AT HIGH ELECTRON EXPOSURE

When hydrated biological materials are irradiated for a longer time than usual, microscopic bubbles begin to appear at random. The first noticeable bubbles appear after the accumulated exposure (for 300 keV electrons) is approximately 150 e/Å^2. At this high exposure, high-resolution features would long since be destroyed, of course, but the macromolecular particles might still be visible. At an earlier point, nascent bubbles or "nuclei" must have been present, but these are presumably too small to be seen in noisy images. The size of bubbles continues to grow with further exposure, soon leaving no trace of the biological macromolecule, but at some point the bubble growth finally stops. An example of the bubbling effect is shown in Fig. 5.

This bubbling effect occurs mainly for biological (and other organic) materials that are hydrated, and even for frozen solutions of small organic molecules such as glycerol. Bubbling is not observed in pure water at liquid nitrogen temperature, whether crystalline or amorphous. With only some

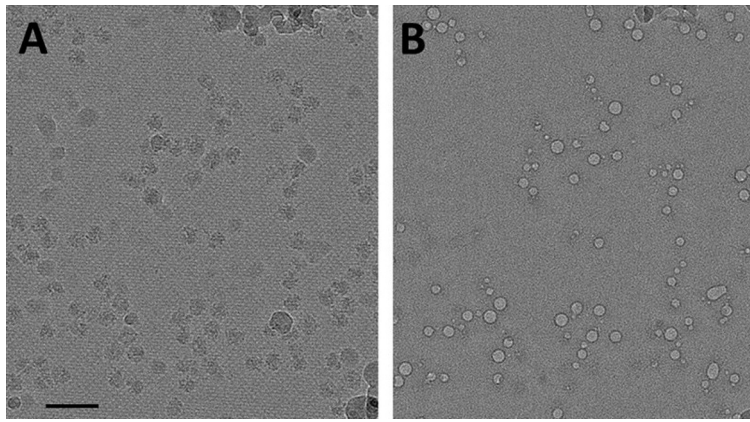

Fig. 5 Example showing the bubbling that occurs in a hydrated biological specimen at very high electron exposure. The specimen in this case consisted of biotinylated 70S ribosomes bound to a streptavidin monolayer crystal, which served as the support film spanning over the open holes of a holey carbon film. The bubbles have a variety of diameters, the largest of which may provide an estimate of the ice thickness. (A) High-resolution image recorded with an exposure of approximately 25 electrons/Å^2. (B) Image recorded after irradiating the sample with a high enough exposure that the growth of bubbles had ceased. Note that much of the globular surface contamination had sublimed at this point, as well. There is a clear correlation between the location of bubbles in (B), and the location of ribosome particles in (A), but not every ribosome particle nucleates a bubble. This image, taken from previously unpublished work using a sample provided by Dr. Arto Pulk, was prepared by Dr. Bong-Gyoon Han.

exceptions, bubbling is also not observed in dry biological materials. The exceptions include very thick organic specimens (eg, plastic sections ~0.5-μm thick), or relatively thick films of carbohydrate materials.

5.1 Bubbles Consist of Molecular Hydrogen

Leapman and Sun used electron energy-loss spectroscopy to identify H_2 gas as the radiolysis product that accumulates in these microscopic bubbles (Leapman & Sun, 1995). More recently, Meents et al. (2010) have also found that H_2 gas accumulates in protein crystals, and in a range of other test samples, when exposed to intense X-ray beams. In this case the gas forms macroscopically visible bubbles when the samples are warmed. Leapman and Sun also went on to estimate that the gas pressure can reach values as high as 1000 atm. At some point the growing bubble touches the surface, and the hydrogen gas suddenly escapes, leaving behind an empty hole in the vitreous ice.

It is not known whether the hydrogen gas is produced within protein, within water, or as a reaction product between the two. Since molecular hydrogen is a radiolysis product both for adjacent $-(CH_2)-$ groups and for pure water, both ought to contribute. What seems more certain is that biological materials appear to serve as nucleation sites for the formation of nascent bubbles, wherever the H_2 gas is first produced.

It is also worth noting that a greater electron exposure may be required in order to eventually observe bubbling at lower dose rates (Brilot et al., 2012; Chen et al., 2008), and the specimen may not show bubbling at all if it is thin enough. In order to account for these effects, it is hypothesized that slower production of H_2 gas, and thinner samples, both increase the chance that hydrogen can escape across the ice surface, and thus not contribute to the formation of bubbles.

5.2 Bubbling Can Be Used to Evaluate the Specimen Thickness

According to the model that bubbles grow until they finally touch the ice-vacuum surface, the largest bubbles would be ones that nucleate near the center of the sample. If this is the case, then the ice thickness can be estimated to be similar to the diameter of the largest bubbles. As an example, the largest bubbles in Fig. 4 are approximately 250 Å in diameter, which is a reasonable value for the thickness of ice-embedded ribosome particles.

5.3 Bubbling Can Be Used to Distinguish Regions with Different Chemical Composition (Bubblegrams)

It has been observed that bubbles form preferentially, and at unusually low electron doses, within the "inner body" protein components of bacterial phage particles (Cheng, Wu, Watts, & Steven, 2014; Wu, Thomas, Cheng, Black, & Steven, 2012). Images that show preferential formation of bubbles, called "bubblegrams," proved to be useful because this effect revealed the location of the inner body, which previously could not be distinguished from the surrounding DNA. In the case of the T7 phage particle, a secondary site of bubbling was also observed, for which bubbles seemed to appear later in the exposure series (Cheng et al., 2014). These studies have also provided information in support of the idea that allowing time for molecular hydrogen to escape the site where it was produced would delay the onset of bubble formation.

6. CRYO-SPECIMENS EXHIBIT COLLECTIVE BEAM-INDUCED MOVEMENT WHEN IRRADIATED

6.1 Radiation-Sensitive Specimens Show Beam-Induced Motion at Quite Low Electron Exposures

It has long been known that adjacent points within local areas of radiation-sensitive specimens move similarly (collectively) when samples are irradiated in the electron microscope. Perhaps the clearest example of collective motion is shown in the behavior of the bend contours exhibited by thin, organic crystals. These bend contours sweep across the face of such crystals well before the electron diffraction pattern itself has faded away. An example documenting such motion is included in a review of radiation damage and electron microscopy of organic polymers by Grubb (1974).

Movement of bend contours reflects a local change in the tilt angle for a given area of a crystalline specimen, such that different areas satisfy one or another Bragg-diffraction condition at different points in time. A dynamic change in the tilt angle does not necessarily mean, however, that there are associated translational shifts in the projected locations of the same points in the crystal.

It has also been suspected that the specimen height of irradiated areas may change relative to the plane of the EM grid. It is well known that the resolution in the image is degraded when a radiation-sensitive specimen is tilted, and this loss of resolution is always in a direction perpendicular to the tilt axis. Furthermore, the resolution is increasingly degraded, the higher the tilt angle. While these facts are easily explained by imagining that a thin crystal bows and flexes as it is irradiated, one cannot rule out the alternative hypothesis that electrostatic charging of the specimen causes the image to be deflected in a direction perpendicular to the tilt axis.

Another observation, which initially suggested the possibility of there being beam-induced specimen movement, was that the high-resolution image contrast is much less than it is expected to be (Henderson & Glaeser, 1985). Crystalline, radiation-sensitive specimens were used in these experiments in order to compare the strength of diffraction spots in the computed Fourier transforms of images to their corresponding strengths in electron diffraction patterns. Once again, the alternative possibility that charging might cause deflection of the image could not be completely ruled out. However, vermiculite, which is expected to become charged as easily as

biological specimens, but which is far less prone to radiation damage, showed considerably higher image contrast, when adjusted for the values of its electron diffraction intensities.

In a recent follow-up to the earlier work, Glaeser, McMullan, Faruqi, and Henderson (2011) showed that images of paraffin could be greatly improved by using much thicker (carbon) support films. The explanation proposed was that the thicker carbon films were much stiffer, and thus they did not deform as easily in response to radiation damage.

The idea to illuminate only a small area of the specimen at a time, referred to as "spot-scan imaging," was introduced as a way to possibly reduce movement of the specimen (Bullough & Henderson, 1987; Downing & Glaeser, 1986). This idea proved to be quite successful, as long as specimens are prepared on continuous carbon films. When specimens are prepared as thin, self-supported films over open holes in the carbon films, however, charging effects severely limit the image quality when the size of the electron beam is smaller than the hole (Brink, Sherman, Berriman, & Chiu, 1998).

As is discussed in Chapter "Direct Electron Detectors" by Henderson and in Chapter "Processing of Cryo-EM Movie Data" by Rubinstein, the development of direct-detection cameras finally made it possible to unambiguously confirm the long-suspected phenomenon of beam-induced movement. More importantly, it also became possible to actually reduce the consequences of this movement by recording images as a series of dose-fractionated "movie frames."

6.2 Thin Cryo-Specimens Undergo Drum-Head-Like Flexing and Doming When Irradiated

One result that influenced thinking greatly, before the advent of direct-detection cameras, was the observation that particles could change their orientation by as much as 2 degree, while low-dose images were being recorded (Henderson et al., 2011). These changes in particle orientation occur as a collective behavior extending over local regions of the specimen, rather than being independent rotations of individual particles. The conclusion was that irradiation causes the thin-film specimen to tilt and bend relative to the plane of the EM grid.

Shortly thereafter, these studies led to recording images as a series of "movie frames" (Brilot et al., 2012). The results that were obtained added the crucial information that the particle rotations are accompanied by translations, both of which vary in magnitude and direction from one part of the field of view to another. In addition, both types of motion occur progressively, as the exposure continues, with the largest movements happening at

the beginning of the exposure. As Brilot et al. then showed, alignment of the images in these frames is effective in compensating for the translational motion that occurs from frame to frame, resulting in better recovery of high-resolution detail.

In at least some cases, the observed particle rotations and translations suggested that the entire irradiated area of the specimen was moving like a drum-head, in effect forming a thin dome (Brilot et al., 2012). Exactly that same type of beam-induced distortion of the specimen had been demonstrated for paraffin crystals by Downing (1988). In the latter case, metal shadowing of the specimen was used to show that in-plane expansion must have occurred in the previously irradiated areas, which resulted in the formation of bulges, or "domes."

6.3 Images Can Be Corrupted Significantly by There Being Changes in *Z*-Height

As noted by Brilot et al. (2012), formation of domes can change the *Z*-height at the center of the field of view by as much as ~20 nm. In addition, we now know—see Chapter "Specimen Preparation for High-Resolution Cryo-EM" by Passmore—that thin-film specimens are susceptible to additional bending and warping, resulting in even greater changes in the *Z*-height within the field of view (Russo & Passmore, 2014). This additional movement, mainly perpendicular to the plane of the grid, happens if precautions are not taken to avoid crinkling of the support film as the sample is cooled, a phenomenon described by Booy and Pawley (1993). When changes in *Z*-height are comparable to the depth of focus for a given resolution, they will produce the same blurring of the image as that produced by idly changing the objective-lens focus, by the same amount, during an exposure. In this context, it is worthwhile to mention that the depth of focus is only 40 nm at a resolution of 4 Å, and just 10 nm at 2 Å resolution.

When the specimen is tilted, changes in *Z*-height (relative to the plane of the grid) also produce a significant component of image motion that is perpendicular to the tilt axis, as was mentioned in Section 6.1. Even for a tilt angle as small as 5 degree, which is difficult to avoid, a 200-Å change of in *Z*-height results in a component of motion perpendicular to the tilt axis that is more than 17 Å.

6.4 The Pattern of Beam-Induced Movement Can Be Quite Unpredictable

As was mentioned in Section 6.2, particle motions are locally correlated, but such motions may differ considerably from one area to another within the

same image. In some cases the differences are symmetric enough to be explained by formation of a dome. In other cases, however, the variation from one area to another can be less simple to describe, almost as when there is turbulent flow. The latter type of locally correlated motion had been demonstrated previously by classifying the Fourier transforms of single particles, a technique introduced by Sander, Golas, and Stark (2003). These classes differed by the amount of motion, even its direction, and by the resolution to which Thon rings extended. When the locations of all particles within a given class was displayed, however, it turned out that members of different classes were grouped together in different areas of a micrograph (Glaeser & Hall, 2011).

Chapter "Processing of Cryo-EM Movie Data" by Rubinstein describes how movies can be processed in a way that accounts for such local correlations in particle motion. While compensating for beam-induced movement in this way is very effective, eliminating such movement to the greatest extent possible remains a top priority. Very significant progress, described in Chapter "Specimen Preparation for High-Resolution Cryo-EM" by Passmore, has been made in developing EM grids that exhibit much less beam-induced movement to begin with, and such grids thus leave less to be compensated by computational methods.

7. MORE THAN ONE MECHANISM MAY CONTRIBUTE TO BEAM-INDUCED MOTION

It is important to remember that the beam-induced particle motions described in Section 6 are actually motions that we observe to occur in the image. Such image motions might reflect mechanical motions that occur in the specimen, of course, but that is not the only possibility. It had long been believed, in fact, that the observed image motion was caused by charging of the specimen, which in turn caused deflection of the electrons as they formed the image. It seems very likely, in fact, that both mechanical motion and image-deflection do happen. Nevertheless, it is still not known how significant the contribution of charging actually is, when care is taken to avoid it as best as one can.

7.1 Cryo-EM Specimens, as Made, Are Expected to Be Under Considerable Stress

It seems certain that cryo-EM specimens, as prepared, are under considerable stress, just as is the case for any glass that has not been subjected to annealing. From a fundamental point of view, we know that the vitreous

state is not one that is at thermodynamic equilibrium. Rather, we have to think of the water molecules as being "frustrated" in their current situation, prevented from getting to a lower-energy state by there being too little thermal energy to get out of the local minimum in which they are trapped.

The frustration referred to above occurs as the water solidifies during rapid cooling. The density of so-called low-density amorphous ice is about 0.94 g/cm^3, which is less than that of super-cooled water (~0.97 g/cm^3) at the temperature of vitrification. It thus is easy to imagine that the expansion that occurs as the solvent solidifies, while everything else is contracting, might result in stress within the vitrified sample.

After solidification occurs, further cooling is expected to generate additional mechanical stress in the sample. This is because the coefficient of thermal expansion for vitreous ice is much greater than that of the EM grid and its support film. As a result, a mismatch in the amount of contraction of these different materials must initially produce unbalanced stress, which, in turn, will deform the thin-foil sample until a static equilibrium is reached. There is also bound to be a mismatch in the thermal contraction behavior of biological samples and the surrounding, vitreous ice. This too might contribute to there being stress in the specimen at the time that it is first prepared.

7.2 Irradiation Can Relieve Mechanical Stress

As is described in Section 2.2, inelastic-scattering events deposit energy in packets that, for the most part, contain between 10 and 100 eV each. This amount of energy is enough to overcome activation barriers and allow local relaxation of stress in the close neighborhood to where the scattering event occurred. When the state of frustration is locally relieved, however, the overall balance of force (stress) changes, and the specimen as a whole can be expected to move by an amount sufficient to restore mechanical equilibrium. This much is only one part of the story, however, since the local input of large packets of energy can also drive a system out of equilibrium, as well as provide energy to overcome the activation barriers that initially serve to frustrate the system from reaching equilibrium.

7.3 Irradiation Can Generate (New) Mechanical Stress

There are multiple ways in which irradiation of cryo-EM specimens can generate stress, which in turn will cause movement (strain) in the specimen. As was pointed out by McBride, Segmuller, Hollingsworth, Mills, and Weber (1986), for example, when a chemical bond is broken, the two atoms involved move apart from a distance of ~1.5 Å to about 3.5 Å, ie, from a

covalent-bond distance to van der Waals contact. More generally, the daughter-molecule products of radiolysis no longer fit into the cavity occupied by the parent molecule. In fact, McBride found that radiolysis of only about 5% of a sample causes the pressure to increase to about half the value that would convert graphite into diamond. Long before that point is reached, however, our thin, foil-like samples will easily bend and buckle in order to prevent the accumulating stress from becoming that large.

As was described in Section 5.1, one of the products of radiolysis in cryo-EM samples is hydrogen gas. Once a bubble of H_2 gas has nucleated, and other molecules of H_2 continue to be produced by further irradiation, the bubbles grow in size. While bubble growth causes obvious specimen motion by displacing adjacent material, visible bubbles only appear at much higher electron exposures than what are used to collect high-resolution data. What is not so obvious is the extent to which nucleation itself already contributes to specimen motion.

7.4 Which Comes First, Relaxation or Creation of Stress?

Beam-induced specimen motion is often observed to occur in two phases, an initial, rapid "burst" phase followed by a slower phase that continues almost indefinitely (see Chapter "Processing of Cryo-EM Movie Data" by Rubinstein and Chapter "Specimen Preparation for High-Resolution Cryo-EM" by Passmore for more about this). Little is known about why the rate of beam-induced movement changes in this way, but two hypotheses seem reasonable. One possibility is that the burst phase reflects the relaxation of stress that had been created during vitrification and subsequent (ie, further) cooling, and the second, slower phase reflects the continuous generation of stress due to radiation damage. A second possibility is that generation of damage-related stress dominates throughout, and any initial relaxation of stress has little to do with beam-induced movement. In this model, it might be hypothesized that beam-induced movement would still be greatest at the beginning, because that is when the specimen experiences the most damage. Later, after almost everything has been damaged, there would be little change in the mechanical stress within the sample.

8. IRRADIATION CAN PRODUCE ELECTROSTATIC CHARGING OF THE SPECIMEN

Irradiation of any specimen by high-energy electrons produces secondary electrons that escape from the surface. If the specimen is an insulator,

as is the case for cyro-EM specimens, it will, as a result, become positively charged. Charging of specimens can, in principle, cause beam-induced movement to occur in two different ways.

One possible mechanism is that electrostatic forces might cause mechanical movement of the specimen. A spot of uncompensated charge on the specimen would be attracted to the nearest conducting surface, the objective aperture or the lens pole piece, for example. Then, since the specimen is a flexible foil, this attractive force would cause bending and warping to occur, just as was described in Section 6. The other possible mechanism is that charging might cause deflection of the image, rather than mechanical motion of the specimen. The two mechanisms are not mutually exclusive, of course, so both may happen simultaneously. It thus is appropriate to describe, a bit further, what is known about the effects of specimen charging, and how to minimize these effects.

8.1 A Buildup of Net Charge on the Specimen Can Be Easy to Detect

Very obvious electron-optical effects occur when an electrically insulating material is put into the electron beam. Examples of such specimens include thin plastic support films and uncoated plastic sections of tissue. Even uncoated biological specimens that are self-supported over holes in a carbon film show strong charging effects when the beam is confined to within the area of the hole.

The effect that is easiest to observe with such specimens is that it can become nearly impossible to focus the unscattered beam in the electron diffraction pattern (Brink, Sherman, et al., 1998; Curtis & Ferrier, 1969). Further, even when the unscattered beam is focused to the best extent possible, moving the specimen by a small amount again causes major distortion of the beam. Looking at the (focused) diffraction pattern is thus a good way to tell whether charging deflects the incident electron beam. In effect, specimen charging can produce an unwanted, additional lens, whose optical quality might be quite nonideal!

8.2 Evidence of Net-Charge Buildup Can Be Reduced in Several Ways

When specimens are prepared on a continuous carbon film, or when they are coated afterward with evaporated carbon, there is no longer any difficulty to focus the diffraction pattern (Brink, Gross, Tittmann, Sherman, & Chiu, 1998), and there is no obvious change in the focused, unscattered beam as

the specimen is moved about. It thus appears that a compensating amount of negative charge is induced in the electrically conductive carbon, matching the positive charge left behind by the escape of secondary electrons (Glaeser & Downing, 2004). The result is to generate an electrostatic-dipole structure rather than an uncompensated, Coulombic charge on the specimen.

It has long been known, as well, that use of an objective aperture reduces specimen charging substantially. The explanation for this effect is that scattered electrons produce low-energy secondary electrons when they hit the aperture. These low-energy electrons are attracted to, and neutralize the positive charge on the surface of the specimen.

Another, commonly used way to minimize charging of uncoated specimens is to include part of the surrounding carbon film within the field that is illuminated by the electron beam. There is compelling evidence that low-energy secondary electrons are once again produced, this time by the surrounding carbon film, and these neutralize the positive charge on the surface of the specimen (Berriman & Rosenthal, 2012). There is also the possibility that the phenomenon of radiation-induced conductivity plays a role in preventing significant specimen charging (Curtis & Ferrier, 1969; Downing, McCartney, & Glaeser, 2004), provided that that the beam illuminates a continuous path between the area of interest and an adjacent part of the carbon support film.

8.3 Other Forms of Specimen Charging Are More Subtle to Detect

There are two additional effects, attributable to specimen charging, which become observable only at low magnification, and then only in highly defocused images. Since it has not been established whether either form contributes to degradation of high-resolution images, it is not known whether these phenomena are things that we need to be concerned about. Still, any form of charging is unwelcome, and thus—for completeness—brief descriptions are included here.

The first effect was initially reported by Dove (1964), who noticed that very low-magnification images of thin carbon films exhibit granular features that fluctuate rapidly in time. Dove coined the phrase "bee swarm" to convey the visual impression that is observed. This effect was then pursued by others including Curtis and Ferrier (1969), who attempted to give a quantitative theoretical explanation of the effect.

The second type of effect was initially described by John Berriman, who noticed that the electron beam can leave an erasable mark on thin carbon films. In the original observations, the irradiated area appeared darker than the surround when the low-magnification image was under-focused, and brighter than the surround when the image was over-focused. This contrast reversal is consistent with the projected Coulomb potential of the irradiated area being more positive than that of the surround. A hallmark of this behavior, sometimes called the "Berriman effect," is that the mark disappears again when an adjacent area of the specimen is irradiated (Downing et al., 2004). This behavior rules out the possibility that the beam-induced mark was due to the well-known buildup of hydrocarbon contamination that occurs when specimens are exposed to intense, focused electron beams at room temperature. A second hallmark of the Berriman effect is the fact that the amount of contrast in the marked location soon saturates. This behavior again differs from what happens in the case of beam-induced contamination, the thickness of which continues to increase the longer the specimen is irradiated.

Further work has found that the radiation-induced mark, while saturable (and thus not due to contamination) is not always erasable (Downing et al., 2004). Operationally, the charging pattern created by irradiating the sample cannot be reversed either by low-energy secondary electrons or by radiation-induced conductivity of adjacent areas.

To complicate things even further, the "Berriman mark" can show the opposite focus-dependent contrast, consistent with the projected Coulomb potential of the irradiated area being less positive (more negative) than that of the surround. The same thing is seen when evaporated carbon films are used to make a "Volta phase plate" for the electron microscope. In this last case it is suggested that the change in projected Coulomb potential reflects a change in the dipole moment per unit area in the region exposed to the intense electron beam, compared to the surround (Danev, Buijsse, Khoshouei, Plitzko, & Baumeister, 2014).

One other point that seems worth mentioning here is that very thin cryo-specimens often show a conventional, dark-contrast "Berriman effect" mark after some tens or hundreds of seconds of exposure, under the same conditions otherwise used for low-dose data collection. This mark on the specimen can be seen in the low-magnification "Search" mode that is used when identifying areas for further data collection. More commonly than not, this mark is seen as a dark ring at the perimeter of the irradiated area (Brink, Sherman, et al., 1998), rather than a uniform, dark disk, as is the case for the original Berriman effect. Thicker cryo-specimens, on the other hand,

do not show such a mark, but instead show the progressive thinning of the irradiated area that is described in Section 4.3. One speculation is that, in regions of thicker ice, positive charge might be more completely carried off by electron-stimulated desorption of ionized water molecules, thereby avoiding the buildup of any significant, positive surface charge.

9. SUMMARY AND FUTURE DIRECTIONS

Vitreous ice and biological macromolecules both sustain extensive amounts of structural damage when irradiated in the electron microscope. It thus has been standard practice to limit the exposure to a "safe" value, ie, not much more than what destroys features of interest.

The ability to record images as a series of movie frames, has established, more clearly than ever before, that significant beam-induced motion occurs long before high-resolution features are fully destroyed. A large component of this beam-induced motion occurs in a direction perpendicular to the plane of the EM grid. A much smaller component is in the plane of the specimen, and—unless compensated by aligning successive movie frames, this smaller component is still large enough to severely limit the image resolution.

Our current ideas of what causes beam-induced movement include the relief of preexisting stress in the specimen as well as progressive generation of (new) stress as the exposure continues. Although specimen charging produces well-known corruption of images, at least the most severe of these effects can be avoided by a number of recommended practices. The extent to which residual specimen charging nevertheless contributes to beam-induced motion, either by generating electrostatic forces or by electron-optical deflection of the image, remains yet to be resolved.

As is described in other chapters of this volume, current research has made significant progress to reduce the amount of beam-induced motion to begin with, and to more effectively recover the signal that would otherwise be lost due to that motion. Nevertheless, mitigation of beam-induced motion remains at the frontier of cryo-EM methodology, and further improvements are bound to be welcome. The ability to prevent local changes in specimen tilt has not yet been addressed, for example. Beam-induced motion may thus continue to be an important issue, especially as the resolution of cryo-EM structures continues to press to ever better values.

ACKNOWLEDGMENTS

It is a pleasure to thank numerous colleagues, especially Kenneth H. Downing, Bong-Gyoon Han, and Richard Henderson, with whom many of the concepts in this chapter, as well as several research papers cited here, have been discussed over many years. Furthermore, I especially want to thank Dr. Greg McMullan for preparing Fig. 4, and Dr. Bong-Gyoon Han for preparing Fig. 5.

REFERENCES

Agard, D., Cheng, Y. F., Glaeser, R. M., & Subramaniam, S. (2014). Single-particle cryo-electron microscopy (cryo-EM): Progress, challenges, and perspectives for further improvement. In P. W. Hawkes (Ed.), *Advances in imaging and electron physics: Vol. 185* (pp. 113–137).

Allen, A. O. (1961). *The radiation chemistry of water and aqueous solutions*. Princeton, NJ: Van Nostrand.

Aronova, M. A., & Leapman, R. D. (2012). Development of electron energy loss spectroscopy in the biological sciences. *MRS Bulletin/Materials Research Society*, *37*(1), 53–62. http://dx.doi.org/10.1557/mrs.2011.329.

Baker, L. A., Smith, E. A., Bueler, S. A., & Rubinstein, J. L. (2010). The resolution dependence of optimal exposures in liquid nitrogen temperature electron cryomicroscopy of catalase crystals. *Journal of Structural Biology*, *169*(3), 431–437. http://dx.doi.org/10.1016/j.jsb.2009.11.014.

Bammes, B. E., Jakana, J., Schmid, M. F., & Chiu, W. (2010). Radiation damage effects at four specimen temperatures from 4 to 100 K. *Journal of Structural Biology*, *169*(3), 331–341. http://dx.doi.org/10.1016/j.jsb.2009.11.001.

Berger, M. J., & Selzer, S. M. (1964). Tables of energy-losses and ranges of electrons and positrons. *Studies in penetration of charged particles in matter* (pp. 205–268). Washington, DC: National Academy of Sciences—National Research Council.

Berriman, J. A., & Rosenthal, P. B. (2012). Paraxial charge compensator for electron cryomicroscopy. *Ultramicroscopy*, *116*, 106–114. http://dx.doi.org/10.1016/j.ultramic.2012.03.006.

Booy, F. P., & Pawley, J. B. (1993). Cryo-crinkling—What happens to carbon-films on copper grids at low-temperature. *Ultramicroscopy*, *48*(3), 273–280.

Brilot, A. F., Chen, J. Z., Cheng, A. C., Pan, J. H., Harrison, S. C., Potter, C. S., … Grigoriefff, N. (2012). Beam-induced motion of vitrified specimen on holey carbon film. *Journal of Structural Biology*, *177*(3), 630–637. http://dx.doi.org/10.1016/j.jsb.2012.02.003.

Brink, J., Gross, H., Tittmann, P., Sherman, M. B., & Chiu, W. (1998). Reduction of charging in protein electron cryomicroscopy. *Journal of Microscopy*, *191*, 67–73.

Brink, J., Sherman, M. B., Berriman, J., & Chiu, W. (1998). Evaluation of charging on macromolecules in electron cryomicroscopy. *Ultramicroscopy*, *72*(1–2), 41–52.

Bullough, P., & Henderson, R. (1987). Use of spot-scan procedure for recording low-dose micrographs of beam-sensitive specimens. *Ultramicroscopy*, *21*(3), 223–229.

Chattarji, D. (1976). *The theory of auger transitions*. London/New York: Academic Press.

Chen, J. Z., Sachse, C., Xu, C., Mielke, T., Spahn, C. M. T., & Grigorieff, N. (2008). A dose-rate effect in single-particle electron microscopy. *Journal of Structural Biology*, *161*(1), 92–100. http://dx.doi.org/10.1016/j.jsb.2007.09.017.

Cheng, N. Q., Wu, W. M., Watts, N. R., & Steven, A. C. (2014). Exploiting radiation damage to map proteins in nucleoprotein complexes: The internal structure of bacteriophage T7. *Journal of Structural Biology*, *185*(3), 250–256. http://dx.doi.org/10.1016/j.jsb.2013.12.004.

Chiu, W., Downing, K. H., Dubochet, J., Glaeser, R. M., Heide, H. G., Knapek, E., … Zemlin, F. (1986). Cryoprotection in electron microscopy. *Journal of Microscopy*, *141*(3), 385–391. http://dx.doi.org/10.1111/j.1365-2818.1986.tb02731.x.

Clark, G. N. I., Hura, G. L., Teixeira, J., Soper, A. K., & Head-Gordon, T. (2010). Small-angle scattering and the structure of ambient liquid water. *Proceedings of the National Academy of Sciences of the United States of America*, *107*(32), 14003–14007. http://dx.doi.org/10.1073/pnas.1006599107.

Cosslett, V. E. (1970). Beam and specimen: Radiation damage and image resolution. *Berichte der Bunsengesellschaft für Physikalische Chemie*, *74*(11), 1171–1175. http://dx.doi.org/10.1002/bbpc.19700741115.

Curtis, G. H., & Ferrier, R. P. (1969). The electric charging of electron-microscopic specimens. *Journal of Physics D: Applied Physics*, *2*(7), 1035–1040. http://dx.doi.org/10.1088/0022-3727/2/7/312.

Danev, R., Buijsse, B., Khoshouei, M., Plitzko, J. M., & Baumeister, W. (2014). Volta potential phase plate for in-focus phase contrast transmission electron microscopy. *Proceedings of the National Academy of Sciences of the United States of America*, *111*(44), 15635–15640.

Dove, D. B. (1964). Image contrasts in thin carbon films observed by shadow electron microscopy. *Journal of Applied Physics*, *35*(5), 1652–1653. http://dx.doi.org/10.1063/1.1713709.

Downing, K. H. (1988). Observations of restricted beam-induced specimen motion with small-spot illumination. *Ultramicroscopy*, *24*(4), 387–398.

Downing, K. H., & Glaeser, R. M. (1986). Improvement in high-resolution image quality of radiation-sensitive specimens achieved with reduced spot size of the electron-beam. *Ultramicroscopy*, *20*(3), 269–278.

Downing, K. H., McCartney, M. R., & Glaeser, R. M. (2004). Experimental characterization and mitigation of specimen charging on thin films with one conducting layer. *Microscopy and Microanalysis*, *10*(6), 783–789.

Garrison, W. M. (1968). Radiation chemistry of organo-nitrogen compounds. In M. Ebert & A. Howard (Eds.), *Current topics in radiation research*: *Vol. 4*. Amsterdam: North-Holand Publishing Company.

Glaeser, R. M., & Downing, K. H. (2004). Specimen charging on thin films with one conducting layer: Discussion of physical principles. *Microscopy and Microanalysis*, *10*(6), 790–796.

Glaeser, R. M., Downing, K., DeRosier, D., Chiu, W., & Frank, J. (2007). *Electron crystallography of biological macromolecules*. Oxford, UK: Oxford University Press.

Glaeser, R. M., & Hall, R. J. (2011). Reaching the information limit in cryo-EM of biological macromolecules: Experimental aspects. *Biophysical Journal*, *100*(10), 2331–2337. http://dx.doi.org/10.1016/j.bpj.2011.04.018.

Glaeser, R. M., McMullan, G., Faruqi, A. R., & Henderson, R. (2011). Images of paraffin monolayer crystals with perfect contrast: Minimization of beam-induced specimen motion. *Ultramicroscopy*, *111*(2), 90–100. http://dx.doi.org/10.1016/j.ultramic.2010.10.010.

Glaeser, R. M., & Taylor, K. A. (1978). Radiation-damage relative to transmission electron-microscopy of biological specimens at low-temperature—Review. *Journal of Microscopy*, *112*, 127–138.

Grant, T., & Grigorieff, N. (2015). Measuring the optimal exposure for single particle cryo-EM using a 2.6 Å reconstruction of rotavirus VP6. *Elife*, *4*, e06980. http://dx.doi.org/10.7554/eLife.06980.

Grimm, R., Typke, D., Barmann, M., & Baumeister, W. (1996). Determination of the inelastic mean free path in ice by examination of tilted vesicles and automated most probable loss imaging. *Ultramicroscopy*, *63*(3–4), 169–179.

Grubb, D. T. (1974). Radiation damage and electron microscopy of organic polymers. *Journal of Materials Science*, *9*(10), 1715–1736. http://dx.doi.org/10.1007/bf00540772.

Hall, E. J., & Giaccia, A. J. (2012). *Radiobiology for the radiologist*. Philadelphia: Wolters Kluwer Health/Lippincott Williams & Wilkins.

Hayward, S. B., & Glaeser, R. M. (1979). Radiation-damage of purple membrane at low-temperature. *Ultramicroscopy*, *4*(2), 201–210.

Heide, H. G. (1984). Observations on ice layers. *Ultramicroscopy*, *14*(3), 271–278. http://dx.doi.org/10.1016/0304-3991(84)90095-0.

Henderson, R. (1990). Cryoprotection of protein crystals against radiation-damage in electron and X-ray-diffraction. *Proceedings of the Royal Society of London. Series B, Biological Sciences*, *241*(1300), 6–8.

Henderson, R., Chen, S. X., Chen, J. Z., Grigorieff, N., Passmore, L. A., Ciccarelli, L., … Rosenthal, P. B. (2011). Tilt-pair analysis of images from a range of different specimens in single-particle electron cryomicroscopy. *Journal of Molecular Biology*, *413*(5), 1028–1046. http://dx.doi.org/10.1016/j.jmb.2011.09.008.

Henderson, R., & Glaeser, R. M. (1985). Quantitative analysis of image contrast in electron micrographs of beam-sensitive crystals. *Ultramicroscopy*, *16*(2), 139–150.

Howells, M. R., Beetz, T., Chapman, H. N., Cui, C., Holton, J. M., Jacobsen, C. J., … Starodub, D. (2009). An assessment of the resolution limitation due to radiation-damage in X-ray diffraction microscopy. *Journal of Electron Spectroscopy and Related Phenomena*, *170*(1–3), 4–12. http://dx.doi.org/10.1016/j.elspec.2008.10.008.

Kempner, E. S. (1993). Damage to proteins due to the direct action of ionizing radiation. *Quarterly Reviews of Biophysics*, *26*(1), 27–48.

Kempner, E. S., & Schlegel, W. (1979). Size determination of enzymes by radiation inactivation. *Analytical Biochemistry*, *92*(1), 2–10. http://dx.doi.org/10.1016/0003-2697(79)90617-1.

Le Caër, S. (2011). Water radiolysis: Influence of oxide surfaces on H2 production under ionizing radiation. *Water*, *3*(1), 235.

Leapman, R. D., & Sun, S. Q. (1995). Cryoelectron energy-loss spectroscopy—Observations on vitrified hydrated specimens and radiation-damage. *Ultramicroscopy*, *59*(1–4), 71–79.

McBride, J. M., Segmuller, B. E., Hollingsworth, M. D., Mills, D. E., & Weber, B. A. (1986). Mechanical stress and reactivity in organic solids. *Science*, *234*(4778), 830–835.

McMullan, G., Vinothkumar, K. R., & Henderson, R. (2015). Thon rings from amorphous ice and implications of beam-induced Brownian motion in single particle electron cryomicroscopy. *Ultramicroscopy*, *158*, 26–32. http://dx.doi.org/10.1010/j.ultramic.2015.05.017.

Meents, A., Gutmann, S., Wagner, A., & Schulze-Briese, C. (2010). Origin and temperature dependence of radiation damage in biological samples at cryogenic temperatures. *Proceedings of the National Academy of Sciences of the United States of America*, *107*(3), 1094–1099. http://dx.doi.org/10.1073/pnas.0905481107.

Ramsier, R. D., & Yates, J. T. (1991). Electron-stimulated desorption: Principles and applications. *Surface Science Reports*, *12*(6–8), 243–378.

Reimer, L., & Kohl, H. (2008). *Transmission electron microscopy physics of image formation*. New York: Springer-Verlag. http://site.ebrary.com/id/10274982.

Ross, F. M. (2015). Opportunities and challenges in liquid cell electron microscopy. *Science*, *350*(6267), 1490. http://dx.doi.org/10.1126/science.aaa9886.

Russo, C. J., & Passmore, L. A. (2014). Ultrastable gold substrates for electron cryomicroscopy. *Science*, *346*(6215), 1377–1380. http://dx.doi.org/10.1126/science.1259530.

Sander, B., Golas, M. M., & Stark, H. (2003). Automatic CTF correction for single particles based upon multivariate statistical analysis of individual power spectra. *Journal of Structural Biology*, *142*(3), 392–401.

Taylor, K. A., & Glaeser, R. M. (1976). Electron microscopy of frozen hydrated biological specimens. *Journal of Ultrastructure Research*, *55*(3), 448–456.

Weik, M., Ravelli, R. B. G., Kryger, G., McSweeney, S., Raves, M. L., Harel, M., … Sussman, J. L. (2000). Specific chemical and structural damage to proteins produced by synchrotron radiation. *Proceedings of the National Academy of Sciences of the United States of America*, *97*(2), 623–628. http://dx.doi.org/10.1073/pnas.97.2.623.

Wright, E. R., Iancu, C. V., Tivol, W. F., & Jensen, G. J. (2006). Observations on the behavior of vitreous ice at ~82 and ~12K. *Journal of Structural Biology*, *153*(3), 241–252. http://dx.doi.org/10.1016/j.jsb.2005.12.003.

Wu, W. M., Thomas, J. A., Cheng, N. Q., Black, L. W., & Steven, A. C. (2012). Bubblegrams reveal the inner body of bacteriophage phi KZ. *Science*, *335*(6065), 182. http://dx.doi.org/10.1126/science.1214120.